Hybrid simulation approaches for induction machine calculation

Georg von Pfingsten, Martin Marco Nell and Kay Hameyer
Institute of Electrical Machines (IEM), RWTH Aachen University, Aachen, Germany

Received 9 January 2018
Revised 3 April 2018
Accepted 9 April 2018

Abstract

Purpose – Induction machines for traction applications are operated at working points of high ferromagnetic saturation. Depending on the working point, a broad spectrum of harmonic frequencies appears in the magnetic flux density of induction machines. Detailed loss analysis therefore requires local and temporal highly resolved nonlinear field computation. This loss analysis can be performed in the post processing of nonlinear transient finite element simulations of the magnetic circuit. However, it takes a large number of transient simulation time steps to build up the rotor flux of the machine.

Design/methodology/approach – In this paper, hybrid simulation approaches that couple static FEA, transient FEA and analytic formulations to significantly decrease the number of simulation time steps to calculate the magnetic field in steady state are discussed, analyzed and compared.

Findings – The proposed hybrid simulation approaches drastically decrease the simulation time by shortening the transient build-up of the rotor flux. Depending on the maximum error of the rotor flux linkage amplitude compared to the steady state value, a reduction of simulation time steps in the range of 55.5 to 98 per cent is found.

Originality/value – The presented hybrid simulation approaches allow efficient performing of the transient FE magnetic field simulations of induction machines operated as traction drives.

Keywords Induction machine, Finite element analysis, Equivalent circuits, Analytic machine models, Model coupling

Paper type Research paper

1. Introduction

In the literature, a variety of model coupling formulations are described. These formulations are used to find the analytical model parameters by FEA and the parameters are subsequently applied in transient analytical models as in the works of Gerber *et al.* (2018) and Roisse *et al.* (1998). Look up tables (LUT) are commonly used to couple multiphysical models with highly different time constant. Chen *et al.* (2015) and Jiang and Jahns (2013) used LUT for the coupling of thermal and magnetic models of permanent magnet synchronous machines. Mohammed *et al.* (2002) used a strong model coupling formulation to study the influence of magnetostriction on a 2-hp drive. Mohammed and Ganu (2010) extracted the lumped parameters from a time harmonic FEA and applied the parameters to a lumped parameter model. In contrast to the model coupling formulations described in the literature, here we use model coupling to reduce the number of time steps of a transient electromagnetic FEA and to pre-estimate the steady state rotor flux linkage values.

Two approaches of coupling transient FEA with static FE models and analytical formulations to a hybrid simulation model are described and assessed in this paper.

Both approaches (Figure 1) rely on the extraction of the lumped parameter matrix $\mathbf{L}$ from static no-load FE simulation (static FEA I). The full inductance matrix $\mathbf{L}$ that contains inductance values L_{ij} between all conductors is extracted from the FE solution as described by Lange *et al.* (2009).

COMPEL - The international journal for computation and mathematics in electrical and electronic engineering
Vol. 37 No. 5, 2018
pp. 1744-1754

0332-1649
DOI 10.1108/COMPEL-01-2018-0015

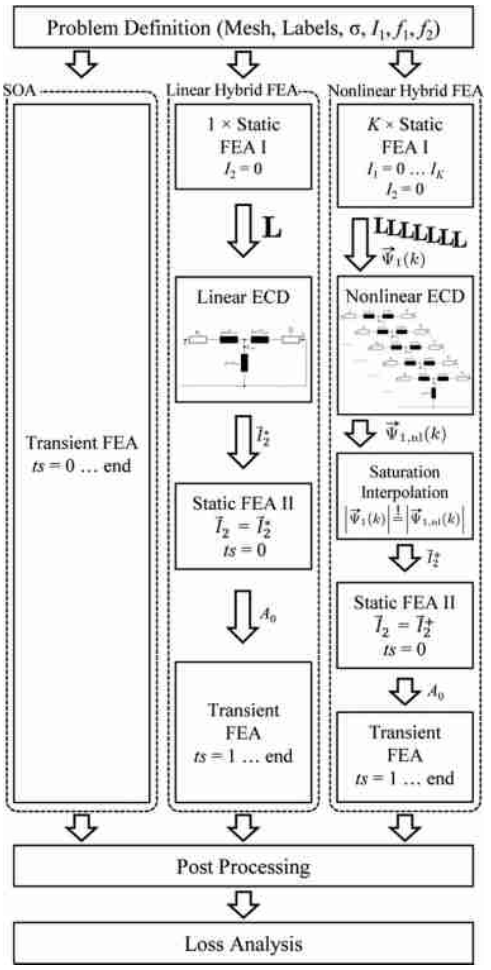

Figure 1.
State of art (SOA) and two different hybrid simulation approaches for reduced simulation effort

Simulating torque-speed operating maps of induction machines from transient FEA is very time consuming (Von Pfingsten *et al.*, 2017a). A large share of computational effort is caused by the transient build-up of the rotor flux. To accelerate this flux build-up in the simulation and save computational time, the steady state flux linkage is calculated from the lumped parameter matrix **L** and the rotor resistance matrix R^2. In the *linear hybrid* approach, one static no-load simulation time step is conducted and one matrix **L** is extracted. The fundamental wave model is parameterized with this matrix **L** and the steady state rotor currents are calculated. As only one saturation state is stored in **L**, the saturation state of the final transient simulation should be known beforehand (Von Pfingsten *et al.*, 2017a). This is easily fulfilled for a linear simulation. For drives operating in different levels of saturation, such as traction drives for electric vehicles (Von Pfingsten *et al.*, 2017b; (Windisch and Hofmann, 2015; Alexandridis *et al.*, 2015), the saturation state is difficult to be estimated beforehand. The *nonlinear hybrid*

approach is introduced, which interpolates the saturation state from multiple matrices $\mathbf{L}$ at different levels of saturation.

2. Hybrid simulation approaches

Both hybrid simulation models use the steady state rotor currents $\vec{I}_2^*$ or $\vec{I}_2^+$, which are calculated from the analytical equivalent circuit diagram, as excitation for the second static FE simulation (FEA II). From the static FEA II, the magnetic vector potential solution A_0 in time step zero is calculated. This solution A_0 is used in the following time step $ts = 1$ as previous solution of the transient time-stepping solution algorithm. From $ts = 2$ on, the transient FE simulation is conducted without any modifications.

For the *linear hybrid* simulation approach, the inductance matrix $\mathbf{L}$ is extracted in the linear case and equation (1) is solved for the two submatrices $\mathbf{L}_{21}$ and $\mathbf{L}_{22}$ of $\mathbf{L}$. As the point of saturation is not interpolated within the *linear hybrid* approach, the rotor currents I_2^* are directly calculated from equation (1) without interpolating the saturation state:

$$\vec{I}_2^* = \left(-\mathrm{j}\cdot\omega_2\cdot\mathbf{L}_{22}(k)+\mathbf{R}_2\right)^{-1}\cdot\left(\mathrm{j}\cdot\omega_2\cdot\mathbf{L}_{21}(k)\cdot\vec{I}_1\right) \tag{1}$$

In the *nonlinear hybrid* simulation approach, the static nonlinear simulation is conducted $k = 1 \ldots K$ times and the full inductance matrix $\mathbf{L}$ is extracted for every of the k simulations. The K full inductance matrices $\mathbf{L}(k)$ is subdivided into four sub-matrices: the self-inductance matrices $\mathbf{L}_{11}(k)$ and $\mathbf{L}_{22}(k)$ and the mutual inductance matrices $\mathbf{L}_{12}(k)$ and $\mathbf{L}_{21}(k)$.

For the *nonlinear hybrid* simulation approach, equation (2) is evaluated for the $k = 1 \ldots K$ different values of $\mathbf{L}$. Each k represents a different saturation state. By solving equation (2), the rotor current I_2 is calculated. I_2 is then inserted to equation (3) to calculate the stator flux linkage vector $\vec{\Psi}_1$. The magnetizing current value $I_{1,\mathrm{nl}}$ at which the stator flux linkage vector $\vec{\Psi}_1$ from equation (3) and the no-load stator flux linkage vector $\vec{\Psi}_{1\mathrm{nl}}$ from equation (4) are equal in length is then found by means of numerical interpolation by equation (5):

$$\vec{I}_2(k) = \left(-\mathrm{j}\cdot\omega_2\cdot\mathbf{L}_{22}(k)+\mathbf{R}_2\right)^{-1}\cdot\left(\mathrm{j}\cdot\omega_2\cdot\mathbf{L}_{21}(k)\cdot\vec{I}_1\right) \tag{2}$$

$$\vec{\Psi}_1(k) = \mathbf{L}_{11}(k)\cdot\vec{I}_1 + \mathbf{L}_{12}(k)\cdot\vec{I}_2(k) \tag{3}$$

$$\vec{\Psi}_{1,\mathrm{nl}}(k) = \mathbf{L}_{11}(k)\cdot\vec{I}_{1,\mathrm{nl}}(k) \tag{4}$$

$$\left\|\vec{\Psi}_1\right\| = \left\|\vec{\Psi}_{1,\mathrm{nl}}\right\| \tag{5}$$

Figure 2 shows the interpolation of the stator flux linkage vectors to find the saturation states for one operating point with a fundamental frequency of the rotor currents of $f_2 = 5$ Hz and different stator excitation peak current density values $\hat{J}_1$. The intersection of the stator flux linkage value $\Psi_{1,\mathrm{nl}}$ (solid black line) and Ψ_1 (colored lines) are marked by black crosses. The black crosses mark the interpolated saturation state. For a frequency of $f_2 = 5$ Hz, the machine is operated in the linear range at stator current density values below $\hat{J}_1 = 5$ A/mm^2. For higher values of stator current density, the machine is operated in a nonlinear case. The saturation is determined not only by the stator current but also by the value of the frequency

f_2. This points out the reason why saturation is not simple to pre-determine and that the interpolation of the saturation state should be applied when simulating induction machine drives that are operated in different saturation states. IMs used as traction motors for electric vehicles are commonly operated at different values of the flux linkage to minimize the machine power losses and to maximize the efficiency of the drive (Von Pfingsten *et al.*, 2017b; Windisch and Hofmann, 2015; Alexandridis *et al.*, 2015). For those machines, the interpolation of the saturation state can help predetermining the steady state using the *nonlinear hybrid* simulation approach.

3. Finite element formulation

The nonlinear time-transient FE formulation is enhanced by the hybrid simulation models (cf. Figure 1). The transient FE formulation is based on a first-order time-stepping equation (6). The algorithm computes a time-dependent function $\boldsymbol{f}$ with time $\boldsymbol{t}$, time step $\boldsymbol{ts}$ and the transient weighting factor $\boldsymbol{\Theta}$ [equation (6)]. The weighting factor $\boldsymbol{\Theta}$ has to comply with (7). Here, $\boldsymbol{\Theta}$ = 2/3 (Galerkin scheme) is used:

$$f(t) = \Theta \cdot f_{ts+1} + (1 - \Theta) \cdot f_{ts} \tag{6}$$

$$0 \leq \Theta \leq 1 \tag{7}$$

The nonlinear field problem is solved by a modified Newton–Raphson procedure. The surface charge density ρ_F is neglected. The following potential formulations are used for the calculation of the transient nonlinear problem [equations (8-10)], with the magnetic vector potential in z-direction A_z, the shape functions α_i and the reluctivity v. In the non-conducting regions (mainly air and electrical steel), equation (8) is used. For the excited windings of the stator, equation (9) is used. For the eddy-current regions (rotor bars), the formulation reads as given in equation (10):

$$\int_{\Omega} \left(\Theta \nabla(\alpha_{i_{ts+1}}) \cdot \nu_{ts+1} \nabla(A_{z_{ts+1}}) \right) d\Omega = \int_{\Omega} \left(-(1 - \Theta) \left(\nabla(\alpha_{i_{ts}}) \cdot \nu_{ts} \nabla(A_{z_{ts}}) \right) \right) d\Omega \tag{8}$$

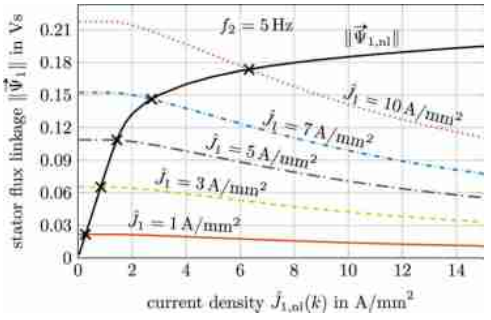

Figure 2.
Interpolation of the stator flux linkage vectors to determine the no-load stator current density $\hat{J}_{1,nl}$ by (5)

$$\int_{\Omega}\left(\Theta\nabla\left(\alpha_{i_{ts+1}}\right)\cdot\nu_{ts+1}\nabla\left(A_{z_{ts+1}}\right)\right)d\Omega$$
$$=\int_{\Omega}\left(-(1-\Theta)\left(\nabla\left(\alpha_{i_{ts}}\right)\cdot\nu_{ts}\nabla\left(A_{z_{ts}}\right)+\Theta\alpha_{i_{ts+1}}\cdot J_{z_{ts+1}}+(1-\Theta)\alpha_{i_{ts}}\cdot J_{z_{ts}}\right)\right)d\Omega \tag{9}$$

$$\int_{\Omega}\left(\Theta\nabla\left(\alpha_{i_{ts+1}}\right)\cdot\nu_{ts+1}\nabla\left(A_{z_{ts+1}}\right)+\alpha_{i_{ts+1}}\cdot\sigma\frac{1}{\Delta t}A_{z_{ts+1}}\right)d\Omega$$
$$=\int_{\Omega}\left(-(1-\Theta)\left(\nabla\left(\alpha_{i_{ts}}\right)\cdot\nu_{ts}\nabla\left(A_{z_{ts}}\right)+\alpha_{i_{ts}}\cdot\sigma\frac{1}{\Delta t}A_{z_{ts}}\right)\right)d\Omega \tag{10}$$

4. Determination of the sampling frequency and mesh density

The sampling frequency f_s of the magnetic field is crucial for the simulation of the iron losses in induction machines. If f_s is chosen that is very small, aliasing reduces the simulated iron losses. For the exemplary studied four-pole machine with $N_1 = 36$ and $N_2 = 28$ rotor slots, a minimum sampling frequency of $f_s = 10$ kHz should be used to prevent aliasing and calculate the correct values of the iron losses (Figure 3). When choosing a sampling frequency that is very small, the local iron losses are not correctly modeled in the laminations in proximity to the air gap, where the magnetic field is most distorted.

Figure 3 illustrates the necessity of simulating the local iron losses using transient FEA. If static FEA is used for the simulation of the local field solution and the iron loss calculation, the influence of current and field displacement of the rotor's current harmonics is neglected. Thus, the local field solution on the surface of the rotor (close to the

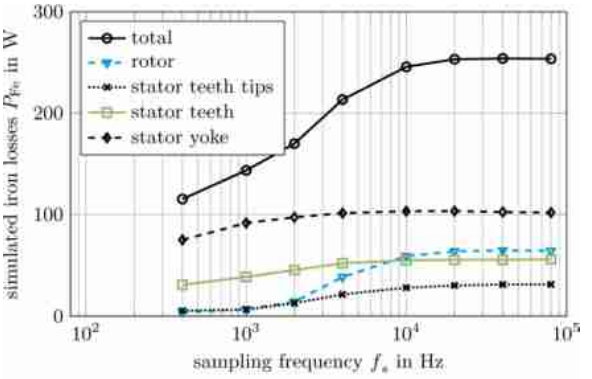

Note: Fundamental frequency $f_1 = 100$ Hz

Figure 3.
Dependency of the simulated iron losses on the sampling frequency f_s of the transient FEA

air-gap) is not correctly modeled and the rotor iron losses cannot be assessed. For induction machines used in electric vehicle traction applications, we found, that the sampling frequency should comply with equation (11) to avoid aliasing.

The mesh density has to be high enough to model the localized harmonics close to the air gap. For the studied 40-kW machine with a maximum speed of 8,000 rpm, the penetration depth of the harmonics in the rotor is less than 0.5 mm. Thus, the mesh size in proximity of the air gap should be less than 0.05 mm. Deeper inside the rotor, the mesh density can be reduced because the change of the magnetic flux density in dependency of time is highly reduced, as the harmonics are damped by the short-circuited rotor bars. As the rotor slots are open, the magnetic field strength inside the electrical steel of the rotor has only minor influence on the skin depth in the rotor bars. Thus, the shape of the rotor slot and the rotor slot opening determines the skin depth and the minimum mesh density:

$$f_s \geq 6 \cdot n \cdot \max(N_1, N_2) \approx 6 \cdot \frac{f_1}{p} \cdot \max(N_1, N_2) \tag{11}$$

5. Results (single operating point)

Figure 4(a) and (b) shows the loci of the complex rotor flux linkage vectors for the state of art method (SOA) and the *nonlinear hybrid* approach for the operating point defined by the

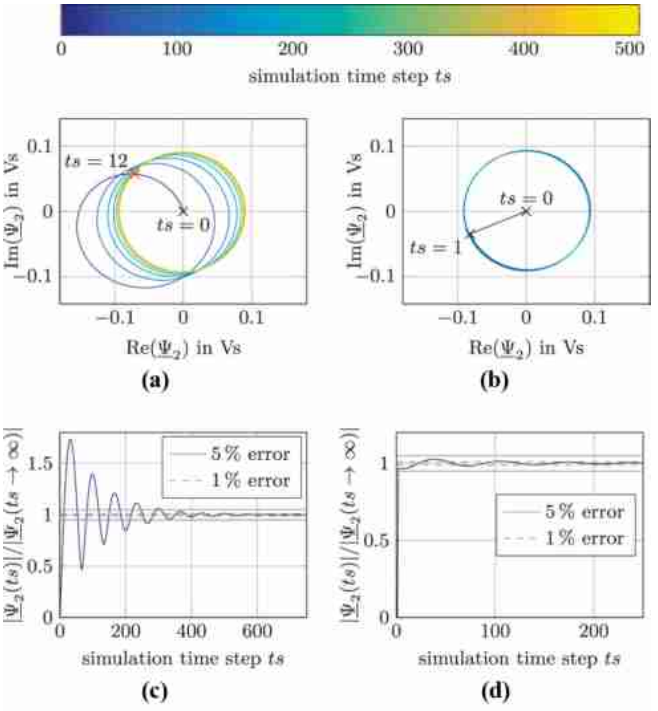

Notes: (a) Zero flux starting condition; (b) with analytical starting condition; (c) zero flux starting condition; (d) with analytical starting condition

Figure 4. Rotor flux loci vector and error in amplitude of rotor flux linkage vector in dependency of simulation time step *ts* for the operating point $\hat{J}_1 = 5\,\mathrm{A/mm^2}$, $f_2 = 5\,\mathrm{Hz}$ with zero flux starting condition (SOA) and with analytical starting condition (*nonlinear hybrid*)

values $\hat{J}_1 = 5\,\mathrm{A/mm^2}$ and $f_2 = 5$ Hz. For the SOA simulation method, the rotor flux linkage shoots over the steady state value in time step $ts = 12$ before settling to the steady state circle [Figure 4(a)]. For the *nonlinear hybrid* approach, it is clearly observed that the rotor flux linkage vector builds up almost instantaneously [Figure 4(b)] and rotates on the steady state circle. Figure 4(c) and (d) shows the instantaneous length of the complex rotor flux linkage vector for SOA and the *nonlinear hybrid* simulation approach. It is observed that the SOA approach takes more than 300 simulation time steps to reach an error of less than 5 per cent, whereas the *nonlinear hybrid* simulation instantaneously reaches an error of less than 5 per cent in time step $ts = 1$.

6. Results (complete operating range)

As it is shown in Von Pfingsten *et al.*'s work (2017b), the complete operating range of an IM used as traction drive for automobile applications can be modeled on a plane spanned by the stator current density $\hat{J}_1$ and the frequency of the rotor currents f_2. The operating points of the 40-kW (peak power) IM range from $\hat{J}_1 = 0 \ldots 10\,\mathrm{A/mm^2}$ and from $f_2 = 0 \ldots 15$ Hz. A total 90 $\left(\hat{J}_1, f_2\right)$ combinations are simulated with a time step of $t_{ts} = 1$ ms. A total of 5,000 time steps are simulated using the nonlinear transient FE simulation for each combination to make sure the steady state is reached. From the last 500 time steps of each of the simulations, the average length of the rotor flux linkage vector is determined according to equation (12) and defined as steady state.

The maximum relative error of the rotor flux linkage $\Delta\Psi_{2,\max}$ is determined for every $\left(\hat{J}_1, f_2\right)$ combination in every simulated time step ts as described in equation (13). The value of $\Delta\Psi_{2,\max}$ is visualized in Figure 5 in dependency of the number of simulated time steps ts:

$$\overline{\Psi}_2\left(\hat{J}_1, f_2\right) = \frac{1}{500} \sum_{ts\,=\,4501}^{5000} \Psi_2\left(\hat{J}_1, f_2, ts\right) \tag{12}$$

$$\Delta\Psi_{2,\max}(\mathrm{ts}) = \max_{\hat{\mathrm{J}}_1, \mathrm{f}_2} \left| \frac{\Psi_2\left(\hat{\mathrm{J}}_1, \mathrm{f}_2, \mathrm{ts}\right) - \overline{\Psi}_2\left(\hat{\mathrm{J}}_1, \mathrm{f}_2\right)}{\overline{\Psi}_2\left(\hat{\mathrm{J}}_1, \mathrm{f}_2\right)} \right|. \tag{13}$$

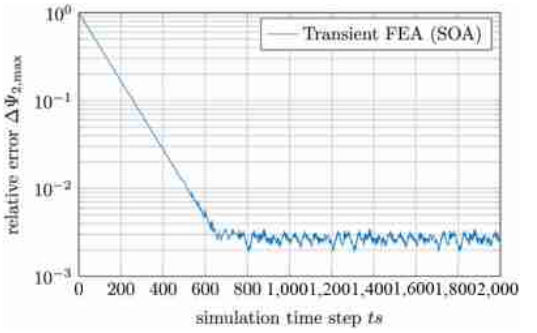

Figure 5.
Maximum relative error of the rotor flux linkage according to equation (5) in dependency of the time step ts

The maximum relative error $\Delta\Psi_{2,\max}$ in Figure 5 exponentially decreases in the first 600 simulation time steps. In the time step $ts = 626$, an error of $\Delta\Psi_{2,\max} \leq 3.5 \times 10^{-3}$ is reached. For simulation time steps larger than $ts > 626$, the error stays in the interval of $1.9 \times 10^{-3} < \Delta\Psi_{2,\max} < 3.5 \times 10^{-3}$. The error of the flux linkage decreases no further. That the error decreases no further are caused by multiple reasons. First, the rotor flux linkage is distorted by harmonics. The harmonics in the rotor conductors have a high frequency and are therefore damped by the short-circuited rotor cage. However, the harmonics of the rotor flux linkage are not damped completely and therefore lead to a difference in length of the rotor flux linkage vector of around 3×10^{-3}. Second, the transient FE simulation has a limited temporal and special resolution and the simulation results therefore are subject to numerical noise. For those reasons, the minimum error value of 3.5×10^{-3} is the minimum error limit of the simulation. A comparison of the different simulation approaches can only be substantive for relative error definition larger than 3.5×10^{-3}.

The transient build-up of the rotor flux linkage reaches steady state after a different number of simulation time steps. In saturated operating points, the steady state is reached in less time steps than in linear operating points. This is underlined by the minimum necessary simulation time steps that are required to reach an error of the rotor flux linkage of $\varepsilon \leq 10 \times 10^{-3}$. Figure 6 shows the minimum number of transient simulation time steps that are required to for the SOA transient simulation in dependency of the stator current density $\hat{J}_1$ and the rotor frequency f_2.

To reach $\varepsilon \leq 10 \times 10^{-3}$ and fulfill equation (15), 28,471 simulation time steps are required in total, which is equal to an average number of time steps of $\overline{ts}_{\varepsilon} = 316.3$ per $\left(\hat{J}_1, f_2\right)$ combination:

$$\Delta\Psi_2\left(\hat{J}_1, f_2, ts\right) = \left| \frac{\Psi_2\left(\hat{J}_1, f_2, ts\right) - \overline{\Psi}_2\left(\hat{J}_1, f_2\right)}{\overline{\Psi}_2\left(\hat{J}_1, f_2\right)} \right| \tag{14}$$

$$ts_{\epsilon}\left(\hat{J}_1, f_2\right) = \min_{ts^*}(ts^*),$$

$$s.t.: \quad \Delta\Psi_2\left(\hat{J}_1, f_2, ts\right) < \epsilon \quad \forall\, ts \geq ts^*. \tag{15}$$

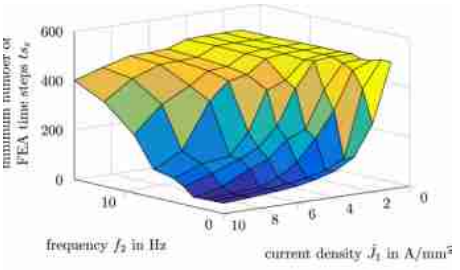

Note: Average number of time steps $ts_{\text{avg}} = 316.3$

Figure 6. Minimum number of simulation time steps to reach an error of less than $\varepsilon \leq 10 \times 10^{-3}$ for the transient FEA (SOA)

In operating points with high values of $\hat{J}_1$ and low values of f_2, the error value of $\varepsilon \leq 10 \times 10^{-3}$ is reached in a lower number of simulation time steps than in operating points with low values of $\hat{J}_1$ or high values of f_2. At $f_2 = 0$ and $\hat{J}_1 = 10\,\mathrm{A/mm^2}$, an error of $\varepsilon \leq 10 \times 10^{-3}$ is reached at $ts_\varepsilon = 42$, whereas at $f_2 = 15$ Hz and $\hat{J}_1 = 1\,\mathrm{A/mm^2}$ $ts_\varepsilon = 506$, simulation time steps are necessary. The $\left(\hat{J}_1, f_2\right)$ combinations where the steady state is reached with a low number of simulation time steps are linked to the operating points that are simulated in saturation. This relation is observed by comparing the stator flux linkage $_1$ in dependency of $\left(\hat{J}_1, f_2\right)$ (Figure 7) and the minimum number of simulation time steps ts_ε (Figure 6).

At an error value of $\varepsilon = 10 \times 10^{-3}$, the *linear hybrid* simulation approach reaches steady state in 8,057 time steps in total and 89.5 time steps in average. The *nonlinear hybrid* simulation approach reaches $\varepsilon = 10 \times 10^{-3}$ in 5,590 simulation time steps, which is equal to an average of 62.1 time steps. Compared to the SOA transient simulation, this is a reduction of simulation time steps of −71.7 per cent (*linear hybrid*) and −80.4 per cent (*nonlinear hybrid*). The reduction of the number of transient simulation time steps by the *nonlinear hybrid* approach over the *linear hybrid* approach is 30.6 per cent.

The minimum number of necessary simulation time steps ts_ε is dependent on the definition of the maximum relative error ε (14,15). A lower value of ε results in a higher number of necessary simulation time steps. Figure 8 presents the average number of necessary time steps $\overline{ts}_\varepsilon$ for the 90 combinations of $\left(\hat{J}_1, f_2\right)$ for the SOA transient FEA and the two hybrid simulation approaches. For the transient FEA, the error ε decreases exponentially with the average number of simulation time steps $\overline{ts}_\varepsilon$. For larger values of ε,

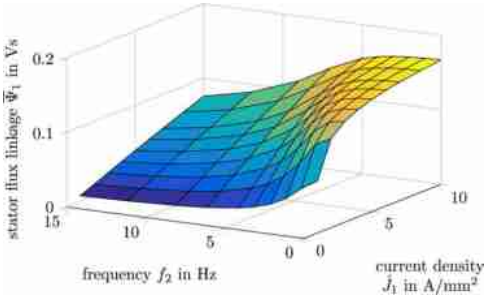

Figure 7.
Length of the steady state stator flux linkage vector in dependency of $\hat{J}_1$ and f_2

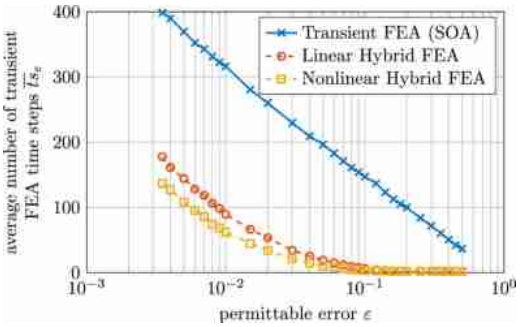

Figure 8.
Average number of time steps $\overline{ts}_\varepsilon$ that is necessary to reach an error of less than ε for the three simulation approaches

the necessary number of simulation time steps to reach steady state is smaller for all three methods. The relative reduction of the necessary number of simulation time steps is drastically reduced by the application of the hybrid simulation approaches. Especially when accepting higher values of ε, the relative advantage increases. For a value of $\varepsilon = 50 \times 10^{-3}$, the total number of simulation steps for the 90 combinations of $(\hat{J}_1, f_2)$ can be reduced from 17,568 (SOA) to 1,602 (*linear hybrid*) and correspondingly 1,215 (*nonlinear hybrid*). If $\varepsilon = 100 \times 10^{-3}$ is acceptable, the total number of simulation time steps can be reduced from 13,140 (SOA) to 477 (*linear hybrid*) and correspondingly 225 (*nonlinear hybrid*). This equals a reduction of simulation time steps of up to 98 per cent. The minimum reduction of the number of simulation time steps is reached at $\varepsilon = 3.5 \times 10^{-3}$ with −55.5 per cent (*linear hybrid*) and −65.8 per cent (*nonlinear hybrid*). These numbers show the advantage of the hybrid simulation approaches. Furthermore, the values of the extracted inductance matrices from the hybrid simulation approaches can be used to simulate the controls of IMs.

This reduction of the transient build-up of the rotor flux linkages is dependent on the rotor time constant T_2. The studied IM has an aluminum rotor cage and a time constant of $T_2 = 110$ ms (linear region). The rotor time constant for short-circuited rotors increases proportional to the rotor inductivity L_2 and decreases with the rotor resistance R^2. Machines with copper cage have a lower rotor resistance and therefore a potentially higher rotor time constant. The law of growth for the magnetic circuit of electric machines indicates, that the rotor inductance L_2 increases stronger with machine size than the rotor resistance R^2. For those reason, IMs in the 5 MW class, such as those applied in wind power turbines, the rotor time constant is several seconds (Boguslawsky *et al.*, 2016). For such larger drives, the reduction of the number of simulation time steps that is necessary for the transient build-up of the rotor flux is expected to be higher than for the 40-kW (peak) IM studied in this paper.

7. Conclusions

Two hybrid simulation approaches that couple static FE simulations with transient FE simulations and analytic formulations are presented. From the SOA transient FE simulation, the minimum difference in the amplitude of the rotor flux linkage vector was identified. The hybrid simulation approaches drastically decrease the simulation time by shortening the transient build-up of the rotor flux. Depending on the maximum error of the rotor flux linkage amplitude compared to the steady state value, a reduction of simulation time steps in the range of −55.5 per cent to −98 per cent was found. For machines larger than the studied 40-kW (peak) IM, the reduction of the number of simulation time steps through the hybrid simulation approaches is expected to be even greater than that analyzed in this paper.

The presented hybrid simulation approaches allow efficient performing of the transient FE magnetic field simulations of induction machines operated as traction drives.

References

Alexandridis, A.T., Konstantopoulos, G.C. and Zhong, Q.C. (2015), "Advanced integrated modeling and analysis for adjustable speed drives of induction motors operating with minimum losses", *IEEE Transactions on Energy Conversion*, Vol. 30 No. 3, pp. 1237-1246.

Boguslawsky, I., Korovkin, N. and Hayakawa, M. (2016), *Large A.C. Machines: Theory and Investigation Methods of Currents and Losses in Stator and Rotor Meshes Including Operation with Nonlinear Loads*, Springer, Japan.

Chen, X., Wang, J. and Griffo, A. (2015), "A high-fidelity and computationally efficient electrothermally coupled model for interior permanent-magnet machines in electric vehicle traction applications", in *IEEE Transactions on Transportation Electrification*, Vol. 1 No. 4, pp. 336-347.

Gerber, M., Gilson, A., Dubas, F. and Espanet, C. (2018), "Coupled circuit and magnetic fast model for high-speed permanent-magnet drive design", *IET Electrical Systems in Transportation*, Vol. 8 No. 1, pp. 27-34.

Jiang, W. and Jahns, T.M. (2013), "Development of efficient electromagnetic-thermal coupled model of electric machines based on finite element analysis", *International Electric Machines & Drives Conference*, *Chicago, IL*, pp. 816-823.

Lange, E., Henrotte, F. and Hameyer, K. (2009), "An efficient field-circuit coupling based on a temporary linearization of FE electrical machine models", *IEEE Transactions on Magnetics*, Vol. 45 No. 3, pp. 1258-1261.

Mohammed, O.A. and Ganu, S. (2010), "FE-circuit coupled model of electric machines for simulation and evaluation of EMI issues in motor drives", *IEEE Transactions on Magnetics*, Vol. 46 No. 8, pp. 3389-3392.

Mohammed, O.A., Calvert, T.E., Petersen, L. and McConnell, R. (2002), "Transient modeling of coupled magnetoelastic problems in electric machines", *IEEE Power Engineering Society Summer Meeting*, *Chicago, IL*, pp. 281-287.

Roisse, H., Hecquet, M. and Brochet, P. (1998), "Simulations of synchronous machines using an electric-magnetic coupled network model", *IEEE Transactions on Magnetics*, Vol. 34 No. 5, pp. 3656-3659.

Von Pfingsten, G., Nell, M. and Hameyer, K. (2017b), "Hybrid simulation methods for induction machine calculation reduction of simulation effort by coupling static FEA with transient FEA and analytic formulations", *18th International Symposium on Electromagnetic Fields in Mechatronics, Electrical and Electronic Engineering (ISEF) Book of Abstracts*, *Lodz*, pp. 1-2.

Von Pfingsten, G., Steentjes, S. and Hameyer, K. (2017a), "Operating point resolved loss calculation approach in saturated induction machines", *IEEE Transactions on Industrial Electronics*, Vol. 64 No. 3, pp. 2538-2546.

Windisch, T. and Hofmann, W. (2015), "Loss minimizing and saturation dependent control of induction machines in vehicle applications", *41st Annual Conference of the IEEE Industrial Electronics Society*, *Yokohama*, pp. 001530-001535.

Corresponding author
Martin Marco Nell can be contacted at: martin.nell@iem.rwth-aachen.de